CRC Assessment Portfolio
Human Studies only

Content

1. Renal haemodynamics

1.1. Determination of renal haemodynamics at baseline by constant-infusion input-clearance technique (PAH, Inulin)

Clearances are performed at the same time in the morning in a quiet and temperature-controlled room. Renal haemodynamics are determined by the constant-infusion input-clearance technique with inulin (Inutest, Fresenius), and sodium p-aminohippurate (PAH) for glomerular filtration rate (GFR) and renal plasma flow (RPF), respectively, as suggested by Cole et al. and repeatedly reported from our laboratory.

After a bolus infusion of inulin and PAH over 15 min and a subsequent constant infusion over 105 min, a steady-state between input and renal excretion of the tracer substances will be reached. Duplicate blood samples will be collected for the assessment of RPF and GFR. PAH is measured according to previously described methods. Inulin is measured indirectly by converting inulin to fructose and subsequently measuring fructose by an enzymatic method (Boehringer Mannheim, Mannheim, Germany). Each blood sample is measured in duplicate with a coefficient variation of <5%.

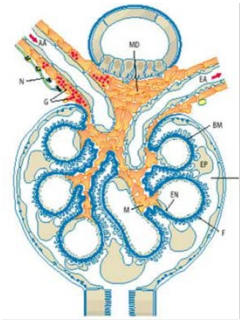

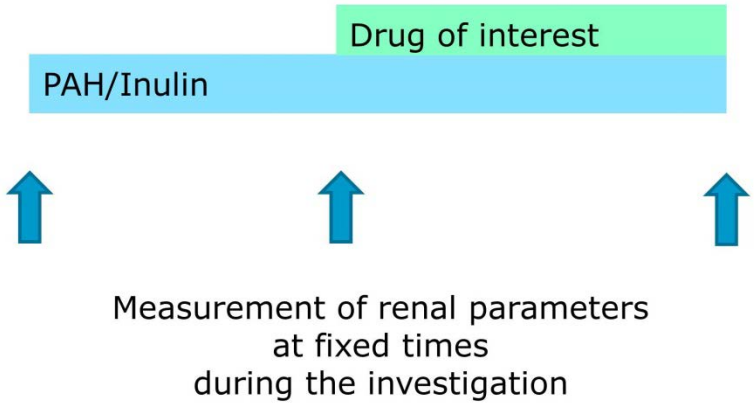

References:

1. Schmieder, RE, Veelken, R, Schobel, H, Dominiak, P, Mann, JF, Luft, FC. Glomerular hyperfiltration during sympathetic nervous system activation in early essential hypertension. **J Am Soc Nephrol.** 1997;8:893-900.
2. Ott, C, Schneider, MP, Raff, U, Ritt, M, Striepe, K, Alberici, M, Schmieder, RE. Effects of manidipine vs. amlodipine on intrarenal haemodynamics in patients with arterial hypertension. **Br J Clin Pharmacol.** 2013;75:129-135.
3. Cole, BR, Giangiacomo, J, Ingelfinger, JR, Robson, AM. Measurement of renal function without urine collection. A critical evaluation of the constant-infusion technic for determination of inulin and para-aminohippurate. **N Engl J Med.** 1972;287:1109-1114.

1.2.Assessment of intraglomerular haemodynamics

RPF and GFR are assessed by applying steady state constant-infusion input-clearance with PAH and Inulin (see 1.1). Filtration fraction (FF) is calculated as GFR/RPF and renal blood flow (RBF) as RPF/(1 – haematocrit). Intraglomerular pressure (P_{glom}) and resistances of the afferent (R_A) and efferent (R_E) arterioles are calculated according to the model originally established by Gomez, which has been discussed by Guidi et al. and applied in previous studies, as follows:

$$\begin{aligned} P_{glom} &= \Delta P_F + P_{Bow} + \pi_G \\ &= (GFR/K_{FG}) + P_{Bow} + (5 \times (C_M - 2)) \\ &= (GFR/K_{FG}) + P_{Bow} + (5 \times ((TP/FF \times \ln(1/1-FF)) - 2)) \end{aligned}$$

In the above equation, K_{FG} (gross filtration coefficient) is estimated as 0.0406 ml s-1 per kidney. P_{Bow} (hydrostatic pressure in the Bowman's space) is estimated as 10 mmHg. π_G (oncotic pressure within glomerular capillaries) can be obtained from C_M (plasma protein concentration within the glomerular capillaries), and calculated from TP (total protein concentration) and FF.

From Ohm's law:

$$R_A = ((MAP - P_{glom})/RBF) \times 1328$$

$$R_E = (GFR/K_{FG} \times (RBF - GFR)) \times 1328$$

References:

1. Ott, C, Schneider, MP, Raff, U, Ritt, M, Striepe, K, Alberici, M, Schmieder, RE. Effects of manidipine vs. amlodipine on intrarenal haemodynamics in patients with arterial hypertension. **Br J Clin Pharmacol.** 2013;75:129-135.
2. Gomez, DM. Evaluation of renal resistances, with special reference to changes in essential hypertension. **J Clin Invest.** 1951;30:1143-1155.
3. Guidi, E, Cozzi, MG, Minetti, EE, Civati, G, Busnach, G, Brando, B. Effect of familial hypertension on glomerular hemodynamics and tubulo-glomerular feedback after uninephrectomy. **Am J Hypertens.** 2001;14:121-128.
4. Delles, C, Klingbeil, AU, Schneider, MP, Handrock, R, Weidinger, G, Schmieder, RE. Direct comparison of the effects of valsartan and amlodipine on renal hemodynamics in human essential hypertension. **Am J Hypertens.** 2003;16:1030-1035.
5. Ott, C, Schlaich, MR, Schmidt, BMW, Titze, SI, Schmieder, RE. Rosuvastatin does not affect intraglomerular haemodynamics in patients with hypercholesterolemia. **J Hypertens.** 2007;25:S17-S17.

1.3. Renal endothelial function (by pharmacologic test)

Renal haemodynamic parameters will be determined by the constant-infusion input-clearance technique with inulin and PAH for GFR and RPF, respectively (see 1.1). After a steady state between input and renal excretion of the tracer substances is reached, the administration of N(G)-monomethyl-L-arginine (L-NMMA) will be started in addition. L-NMMA is administered intravenously as a bolus infusion (3 mg/kg over 5 min) followed by constant infusion (2 mg/kg over 30 min). Thus, the total dose of L-NMMA will be 4.25 mg/kg.

The change in RPF in response to L-NMMA served as a measure of basal nitric oxide (NO) activity in the renal circulation. The magnitude of the vasoconstrictive response to the blockade of NO synthesis mirrors the vasodilatory effect of NO at baseline in the renal endothelium. Thus, a greater vasoconstrictive response after L-NMMA application indicates a greater blockade of NO.

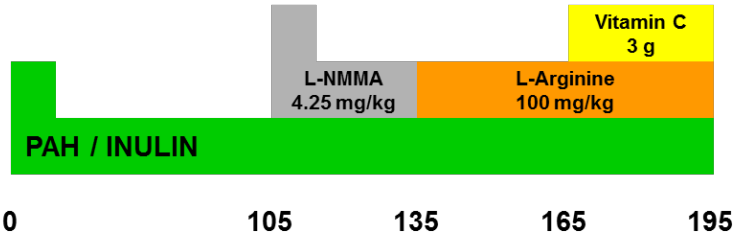

Then L-arginine (L-arginine hydrochloride 6% total dose 100mg/kg given over 30 min) will be administered to counteract the L-NMMA induced vasoconstriction, and hence returning to baseline levels is negligible. The dose of L-arginine is so low that the effect related to the infusion of an aminoacid occurs. Finally, co-infusion of vitamin C a total dose of 3 g over 30 minutes will be started (during continued infusion of L-arginine), to assess the contribution of oxidative stress to NO bioavailability in the renal vasculature

In addition, urine and blood samples taken at the end of each treatment phase will be secured in order to measure tubular markers and inflammatory parameters.

<u>Risk measuring renal endothelial function and using clearance techniques:</u>

Intravenous administration of L-NMMA normally increases blood pressure (BP). However, only patients without or with arterial hypertension grade 1 or 2 are included. Therefore, hypertensive crisis is most unlikely and have never occurred in our hands. Nevertheless, BP is monitored closely throughout the intravenous administration of L-NMMA. If nevertheless the systolic BP rises over 200 mmHg or the diastolic BP rises over 110 mmHg, intravenous administration will be stopped. No other side effects of intravenous administration of L-NMMA were observed in over 800 measurements in the last 15 years, carried out in a variety of patient populations. For safety reason, we infuse intravenous L-arginine (L-arginine hydrochloride 6%) to counteract possible prolonged L-NMMA induced vasoconstriction. L-arginine is an acid solution, which can damage surrounding tissue, if it is given para-venously. Therefore, it is checked if the intravenous line lies correct and hence L-arginine is administered strictly intravenous. Vitamin C infusion (in the current dosage) has no (known) additional adverse effects.

References:

1. Schmieder, RE, Veelken, R, Schobel, H, Dominiak, P, Mann, JF, Luft, FC. Glomerular hyperfiltration during sympathetic nervous system activation in early essential hypertension. **J Am Soc Nephrol.** 1997;8:893-900.

2. Ott, C, Schlaich, MP, Schmidt, BM, Titze, SI, Schaufele, T, Schmieder, RE. Rosuvastatin improves basal nitric oxide activity of the renal vasculature in patients with hypercholesterolemia. **Atherosclerosis.** 2008;196:704-711.
3. Schneider, MP, Schneider, A, Jumar, A, Kistner, I, Ott, C, Schmieder, RE. Effects of folic acid on renal endothelial function in patients with diabetic nephropathy: results from a randomized trial. **Clin Sci (Lond).** 2014;127:499-505.
4. Friedrich, S, Schmieder, RE. Review of direct renin inhibition by aliskiren. **J Renin Angiotensin Aldosterone Syst.** 2013;14:193-196.
5. Jacobi, J, Schneider, MP, John, S, Schmieder, RE. Impact of NO-synthase inhibition on renal hemodynamics in normotensive and hypertensive subjects. **J Hypertens.** 2002;20:525-530.
6. Delles, C, Jacobi, J, John, S, Fleischmann, I, Schmieder, RE. Effects of enalapril and eprosartan on the renal vascular nitric oxide system in human essential hypertension. **Kidney Int.** 2002;61:1462-1468.
7. Delles, C, Jacobi, J, Schlaich, MP, John, S, Schmieder, RE. Assessment of endothelial function of the renal vasculature in human subjects. **Am J Hypertens.** 2002;15:3-9.
8. Delles, C, Schneider, MP, Oehmer, S, Fleischmann, I, Fleischmann, EF, Schmieder, RE. Increased response of renal perfusion to the antioxidant vitamin C in type 2 diabetes. **Nephrol Dial Transplant.** 2004;19:2513-2518.
9. Schlaich, MP, Jacobi, J, John, S, Delles, C, Fleischmann, I, Schmieder, RE. Is l-arginine infusion an adequate tool to assess endothelium-dependent vasodilation of the human renal vasculature? **Clin Sci (Lond).** 2000;99:293-302.
10. Ott, C, Kistner, I, Keller, M, Friedrich, S, Willam, C, Bramlage, P, Schmieder, RE. Effects of linagliptin on renal endothelial function in patients with type 2 diabetes: a randomised clinical trial. **Diabetologia.** 2016;59:2579-2587.

2. Central Haemodynamics and vascular (endothelial) function

2.1.Impedance cardiography

Bioimpedance cardiography allows non-invasive, continuous measurement of central haemodynamics (stroke volume, cardiac output, heart rate, total peripheral resistance). The measuring principle of electrical bioimpedance cardiography is based on the varying flux intensity and frequency at the base of the thorax originating from skin electrodes. The same alternating flow is recovered at the neck base by further electrodes. The continuous flow through the fluid media of the thorax allows recording of the electrical impedance of the thorax and its changes during a cardiac cycle. From this, beat and cardiac output are calculated.

Bioimpedance cardiography is available in the CRC for years and has been used in several clinical trials. In particular, changes in a series of experiments are highly valid and reliable.

References:

1. Siedlecka, J, Siedlecki, P, Bortkiewicz, A. Impedance cardiography - Old method, new opportunities. Part I. Clinical applications. **Int J Occup Med Environ Health.** 2015;28:27-33.
2. Fellahi, JL, Fischer, MO. Electrical bioimpedance cardiography: an old technology with new hopes for the future. J Cardiothorac **Vasc Anesth.** 2014;28:755-760.
3. Schmieder, RE, Schobel, HP, Gatzka, CE, Hauser, W, Dominiak, P, Mann, JF, Luft, FC. Effects of angiotensin converting enzyme inhibitor on renal haemodynamics during mental stress. **J Hypertens.** 1996;14:1201-1207.
4. Reinold, A, Schneider, A, Kalizki, T, Raff, U, Schneider, MP, Schmieder, RE, Schmidt, BMW. Increased Aldosterone Release During Head-Up Tilt in Early Primary Hypertension. **Am J Hypertens.** 2017;30:484-489.

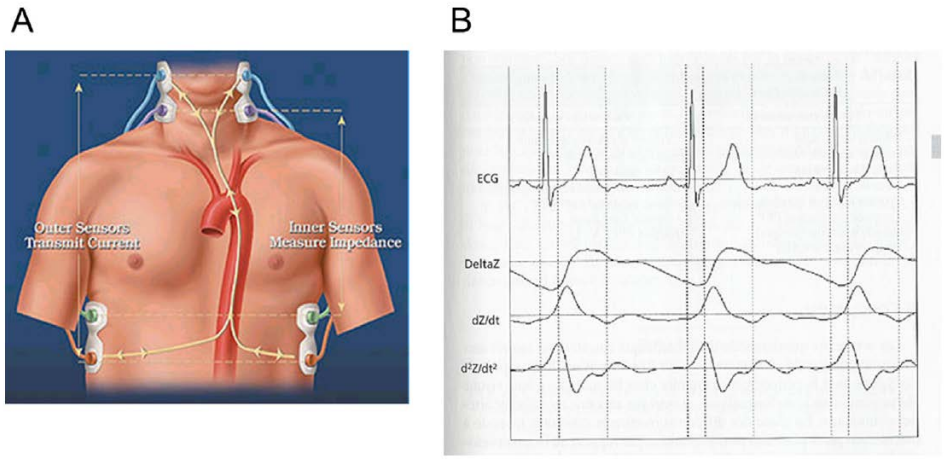

2.2.Flow mediated vasodilation (by UNEX EF)

Flow mediated vasodilation (FMD) will be measured according to international standards. FMD is determined as the dilation of the brachial artery after 5 minutes of forearm ischemia, induced by inflation of a BP cuff on the upper arm to suprasystolic levels. FMD in healthy subjects is $\geq$ 5%, but more detailed gender-specific reference values for different age groups have been published. A large number of studies have shown its predictive value, even in unselected population based studies.

Assessment of FMD of the brachial artery by a semi-automatic ultrasound system using an H-type ultrasound probe represents a new development that overcomes the limitation of classic systems

(in particular the investigator-dependency of conventional, “hand-held” FMD measurements). This system comprised a 7.5-MHz linear array transducer and a novel stereotactic probe-holding device (UNEX EF 18G; Unex Co., Nagoya, Japan). This novel semi-automatic assessment of FMD has been shown to improve the precision and repeatability of the measurements. With this more precise method, it is now also possible to measure the low flow mediated vasoconstrictor (L-FMC) response of the brachial artery that accompanies the cuff inflation period. Data have shown that the combined assessment of FMD+L-FMC, i.e. the flow mediated total dilation (FMTD) further improves characterization of underlying vascular disease.

In brief, continuous recordings of B-mode images and A-mode waves of the brachial artery in the longitudinal plane will be obtained. A segment with clear near (media-adventitia) and far (intima-inner lumen) interfaces will be manually determined. These border interfaces will be identified automatically based on the A-mode waves, and the diastolic diameter of the brachial artery per beat will be synchronized with the ECG R-wave and tracked automatically. The right brachial artery will be scanned in longitudinal sections 1–10 cm above the elbow, the skin surface will be marked and the arm will be kept in the same position during the study. A pneumatic cuff placed around the forearm will be inflated for 5 min to at least 50 mmHg above systolic pressure. The diameter of the brachial artery will be scanned and recorded at baseline before cuff inflation, and continuously from the release point to 2 min after cuff deflation to obtain the maximum diameter during reactive hyperemia. The diameter of the artery will be measured from one media–adventitia interface to the other at end-diastole, coincident with the R-wave on the continuously recorded electrocardiogram. L-FMC will be calculated from the mean arterial diameter during the last 30 s before cuff release and expressed as percentage change from baseline. Traditional FMD will be calculated as the maximum percent increase in arterial diameter during continuous measurement of arterial diameter in the 4.5 min following cuff deflation. Finally FMTD as a composite endpoint will be calculated as the sum of the absolute values of FMD and L-FMC. The artery diameter will be recorded in the same manner at 15 sec interval after the first measurement and at 60-sec intervals after the second measurement. All data will be analyzed in a randomized, blinded fashion.

References:

1. Corretti, MC, Anderson, TJ, Benjamin, EJ, Celermajer, D, Charbonneau, F, Creager, MA, Deanfield, J, Drexler, H, Gerhard-Herman, M, Herrington, D, Vallance, P, Vita, J, Vogel, R, International Brachial Artery Reactivity Task, F. Guidelines for the ultrasound assessment of endothelial-dependent flow-mediated vasodilation of the brachial artery: a report of the International Brachial Artery Reactivity Task Force. **J Am Coll Cardiol.** 2002;39:257-265.
2. Tomiyama, H, Kohro, T, Higashi, Y, Takase, B, Suzuki, T, Ishizu, T, Ueda, S, Yamazaki, T, Furumoto, T, Kario, K, Inoue, T, Koba, S, Watanabe, K, Takemoto, Y, Hano, T, Sata, M, Ishibashi, Y, Node, K, Maemura, K, Ohya, Y, Furukawa, T, Ito, H, Ikeda, H, Yamashina, A. Reliability of measurement of endothelial function across multiple institutions and establishment of reference values in Japanese. **Atherosclerosis.** 2015;242:433-442.

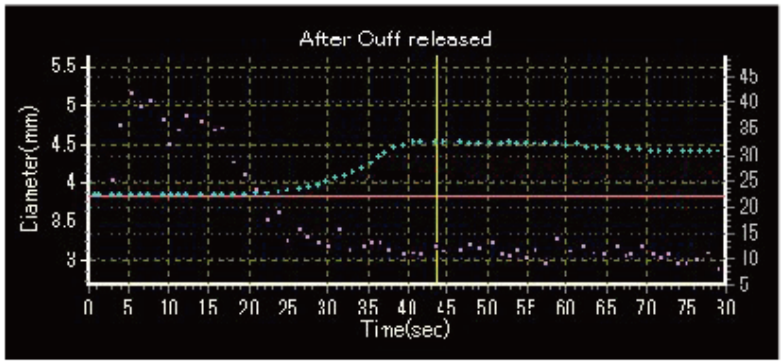

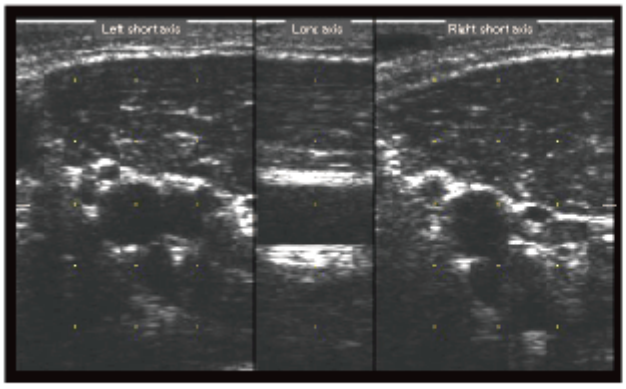

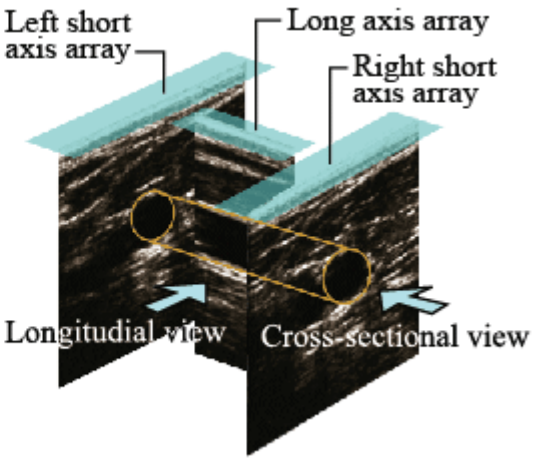

3. Shechter, M, Shechter, A, Koren-Morag, N, Feinberg, MS, Hiersch, L. Usefulness of Brachial Artery Flow-Mediated Dilation to Predict Long-Term Cardiovascular Events in Subjects Without Heart Disease. **American Journal of Cardiology.** 2014;113:162-167.
4. Yeboah, J, Folsom, AR, Burke, GL, Johnson, C, Polak, JF, Post, W, Lima, JA, Crouse, JR, Herrington, DM. Predictive Value of Brachial Flow-Mediated Dilation for Incident Cardiovascular Events in a Population-Based Study The Multi-Ethnic Study of Atherosclerosis. **Circulation.** 2009;120:502-509.
5. Yeboah, J, McClelland, RL, Polonsky, TS, Burke, GL, Sibley, CT, O'Leary, D, Carr, JJ, Goff, DC, Greenland, P, Herrington, DM. Comparison of Novel Risk Markers for Improvement in Cardiovascular Risk Assessment in Intermediate-Risk Individuals. **Jama-Journal of the American Medical Association.** 2012;308:788-795.
6. Kabutoya, T, Hoshide, S, Ogata, Y, Iwata, T, Eguchi, K, Kario, K. The time course of flow-mediated vasodilation and endothelial dysfunction in patients with a cardiovascular risk factor. **Journal of the American Society of Hypertension.** 2012;6:109-116.
7. Iguchi, T, Takemoto, Y, Shimada, K, Matsumoto, K, Nakanishi, K, Otsuka, K, Hyodo, E, Hirohashi, K, Tahara, A, Yoshiyama, M. Simultaneous assessment of endothelial function and morphology in the brachial artery using a new semiautomatic ultrasound system. **Hypertension Research.** 2013;36:691-697.
8. Norioka, N, Takemoto, Y, Kobayashi, M, Makuuchi, A, Yoshikawa, J, Yamazaki, Y, Kamiyama, Y, Shuto, T, Yoshiyama, M. Low-flow mediated constriction incorporated indices as indicators of cardiovascular risk in smokers. **Atherosclerosis.** 2016;251:132-138.

2.3.Pulse wave analysis and Pulse wave velocity

Pulse wave analysis

To derive the central arterial waveform, a validated system (SphygmoCor™ System) will be used. Brachial BP will be measured with an oscillometric device (e.g. Dinamap Pro 100V2) and averages of the last three measurements will be taken. Immediately thereafter, radial artery waveforms will be recorded from the radial artery at the wrist, using high-fidelity applanation tonometer, directly into the SphygmoCor™ System. Radial artery waveform will be averaged from single waveforms recorded consecutively for 8 seconds. Corresponding central (aortic) waveform is then automatically generated from the radial artery waveform by a validated transfer function. From the derived central waveforms, data are given on central systolic and diastolic pressure, central pulse pressure, central augmentation pressure and central augmentation index. The central augmentation index will also be normalized to a heart rate of 75 beats per minute. Therefore, different baseline levels of heart rate or changes in heart rate due to provocative manoeuvres, do not contribute to changes in central augmentation index. In addition, data about forward and backward wave amplitude will be given.

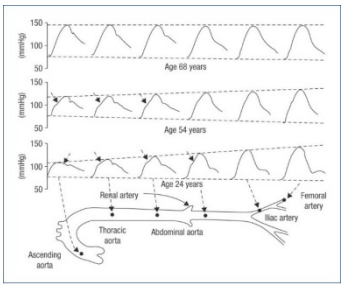

Fig. 1 – Aortic pressure can differ significantly from brachial pressure and individuals with the same brachial pressure can have significantly different aortic pressures*

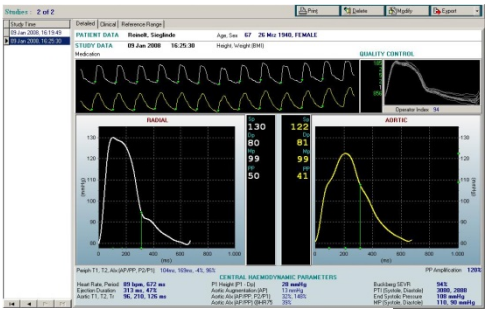

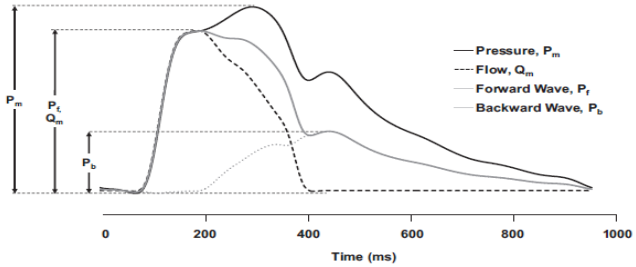

Pulse wave velocity:

Aortic PWV will be determined using the foot-to-foot methods with a validated System (SphygmoCor™ XCEL System).

References:

1. Ott, C, Raff, U, Harazny, JM, Michelson, G, Schmieder, RE. Central pulse pressure is an independent determinant of vascular remodeling in the retinal circulation. **Hypertension.** 2013;61:1340-1345.
2. Ott, C, Raff, U, Schmidt, S, Kistner, I, Friedrich, S, Bramlage, P, Harazny, JM, Schmieder, RE. Effects of saxagliptin on early microvascular changes in patients with type 2 diabetes. **Cardiovascular Diabetology.** 2014;13:19.

3. Ott, C, Schmid, A, Toennes, SW, Ditting, T, Veelken, R, Uder, M, Schmieder, RE. Central pulse pressure predicts BP reduction after renal denervation in patients with treatment-resistant hypertension. **EuroIntervention.** 2015;11:110-116.
4. Ott, C, Jumar, A, Striepe, K, Friedrich, S, Karg, MV, Bramlage, P, Schmieder, RE. A randomised study of the impact of the SGLT2 inhibitor dapagliflozin on microvascular and macrovascular circulation. **Cardiovascular Diabetology.** 2017;16:26.
5. Striepe, K, Jumar, A, Ott, C, Karg, MV, Schneider, MP, Kannenkeril, D, Schmieder, RE. Effects of the Selective Sodium-Glucose Cotransporter 2 Inhibitor Empagliflozin on Vascular Function and Central Hemodynamics in Patients With Type 2 Diabetes Mellitus. **Circulation.** 2017;136:1167-1169.
6. Raff, U, Walker, S, Ott, C, Schneider, MP, Schmieder, RE. Olmesartan improves pulse wave velocity and lowers central systolic blood pressure and ambulatory blood pressure in patients with metabolic syndrome. **J Clin Hypertens (Greenwich).** 2015;17:98-104.
7. Karamanoglu, M, O'Rourke, MF, Avolio, AP, Kelly, RP. An analysis of the relationship between central aortic and peripheral upper limb pressure waves in man. **Eur Heart J.** 1993;14:160-167.
8. Wilkinson, IB, Fuchs, SA, Jansen, IM, Spratt, JC, Murray, GD, Cockcroft, JR, Webb, DJ. Reproducibility of pulse wave velocity and augmentation index measured by pulse wave analysis. **J Hypertens.** 1998;16:2079-2084.
9. Pauca, AL, O'Rourke, MF, Kon, ND. Prospective evaluation of a method for estimating ascending aortic pressure from the radial artery pressure waveform. **Hypertension.** 2001;38:932-937.

2.4. Twenty-four-hour ambulatory BP and ambulatory vascular stiffness

Measurement of 24-h ambulatory BP (central and brachial) as well as vascular parameters under ambulatory conditions will be done with a commercially available and routinely used ABPM system (Mobilograph ™, IEM, Stollberg, Germany) that has been validated.

Reference:

1. Striepe, K, Jumar, A, Ott, C, Karg, MV, Schneider, MP, Kannenkeril, D, Schmieder, RE. Effects of the Selective Sodium-Glucose Cotransporter 2 Inhibitor Empagliflozin on Vascular Function and Central Hemodynamics in Patients With Type 2 Diabetes Mellitus. **Circulation.** 2017;136:1167-1169.
2. Papaioannou, TG, Argyris, A, Protogerou, AD, Vrachatis, D, Nasothimiou, EG, Sfikakis, PP, Stergiou, GS, Stefanadis, CI. Non-invasive 24 hour ambulatory monitoring of aortic wave reflection and arterial stiffness by a novel oscillometric device: the first feasibility and reproducibility study. **Int J Cardiol.** 2013;169:57-61.
3. Weber T, Wassertheurer S, Schmidt-Trucksäss A, Rodilla E, Ablasser C, Jankowski P, Lorenza Muiesan M, Giannattasio C, Mang C, Wilkinson I, Kellermair J, Hametner B, Pascual JM, Zweiker R, Czarnecka D, Paini A, Salvetti M, Maloberti A, McEniery C. Relationship Between 24-Hour Ambulatory Central Systolic Blood Pressure and Left Ventricular Mass: A Prospective Multicenter Study. **Hypertension.** 2017;70:1157-1164.

3. Retinal haemodynamics

3.1. Retinal capillary flow

To assess retinal vessels scanning laser Doppler flowmetry (SLDF) at 670 nm (Heidelberg Retina Flowmeter, Heidelberg Engineering, Germany) will be performed. The confocal technique of the device will ensure that only capillary blood flow of the superficial layer of 300µm will be measured.

For perfusion analysis, capillary vessels with a diameter of more than 20 µm are selected and perfusion in these capillaries are not respected in the blood flow calculation of retinal capillary flow. This process is performed using the automatic full field perfusion image analyser (AFFPIA). The methods of SLDF and AFFPIA have been extensively described in previous studies.

Retinal capillary flow will be measured after 30 minutes of rest (baseline) and after flicker light stimulation (10Hz; Photo Stimulator 750, Siemens-Elema AB, Germany) to assess endothelium dependent changes in retinal capillary flow. Flickering light increases retinal blood flow at least in part via a NO-dependent mechanism and represents a non-pharmacological tool to investigate vasodilatory capacity of retinal capillaries. Diffuse luminance flicker has no effects on systemic BP, thereby minimizing potential systemic hemodynamic influences on retinal capillary flow.

In addition, also individual pulsatile pattern of RCF of retinal arterioles in systole and diastole can be reliably assessed.

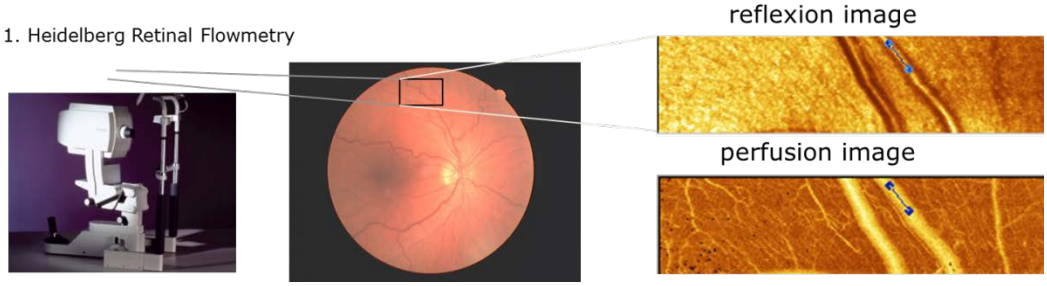

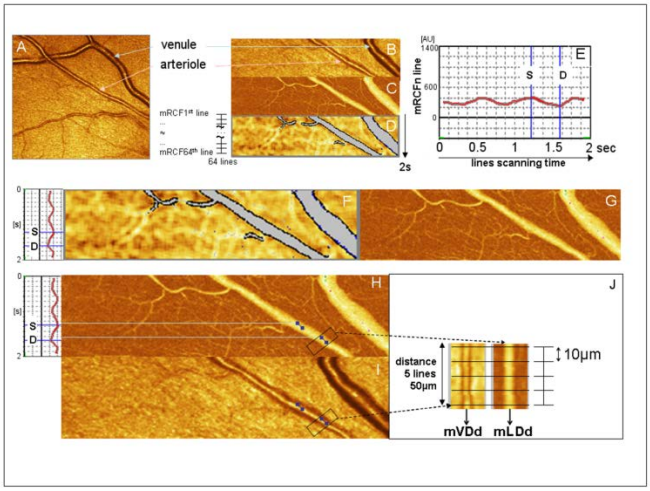

Reference:

1. Harazny, JM, Ott, C, Raff, U, Welzenbach, J, Kwella, N, Michelson, G, Schmieder, RE. First experience in analysing pulsatile retinal capillary flow and arteriolar structural parameters measured noninvasively in hypertensive patients**. J Hypertens.** 2014;32:2246-2252.
2. Delles, C, Michelson, G, Harazny, J, Oehmer, S, Hilgers, KF, Schmieder, RE. Impaired endothelial function of the retinal vasculature in hypertensive patients. **Stroke.** 2004;35:1289-1293.
3. Michelson, G, Warntges, S, Harazny, J, Oehmer, S, Delles, C, Schmieder, RE. Effect of nos inhibition on retinal arterial and capillary circulation in early arterial hypertension. Retina. 2006;26:437-444.
4. Ritt, M, Harazny, JM, Ott, C, Raff, U, Bauernschubert, P, Lehmann, M, Michelson, G, Schmieder, RE. Impaired increase of retinal capillary blood flow to flicker light exposure in arterial hypertension. **Hypertension.** 2012;60:871-876.
5. Ritt, M, Harazny, JM, Schmidt, S, Raff, U, Ott, C, Michelson, G, Schmieder, RE. Haemoglobin and vascular function in the human retinal vascular bed. **J Hypertens.** 2013;31:775-781.
6. Kreis, AJ, Nguyen, T, Rogers, S, Wang, JJ, Harazny, J, Michelson, G, Farouque, HM, Wong, TY. Reliability of different image analysis methods for scanning laser Doppler flowmetry. **Curr Eye Res.** 2008;33:493-499.
7. Bosch, AJ, Harazny, JM, Kistner, I, Friedrich, S, Wojtkiewicz, J, Schmieder, RE. Retinal capillary rarefaction in patients with untreated mild-moderate hypertension. **BMC Cardiovasc Disord.** 2017;17:300.

3.2.Retinal vascular remodeling

By using SLDF, also structural parameters of retinal arterioles can be assessed with high reliability.

In brief, outer arteriolar diameter (OD) is measured in reflection images, and inner (lumen) diameter (ID) is assessed in perfusion images (software version SLDF 4.0). WLR is determined using the formula (OD-ID)/ID, wall thickness (WT) is calculated using the formula OD – ID/2 and cross-sectional area (CA) is determined using the formula 3.14 x (OD [5] – ID [5])/4.

Similar to our retinal capillary flow analysis (see 3.1), also structural parameters can be assessed according to different heart phases (systole and diastole).

Reliability of SLDF measurement has been previously shown to be fair (coefficient of variation <10%).

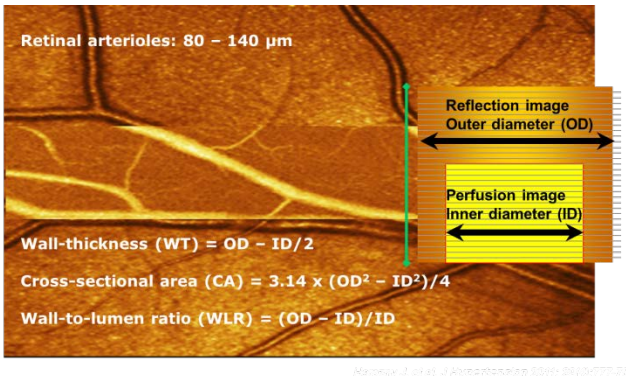

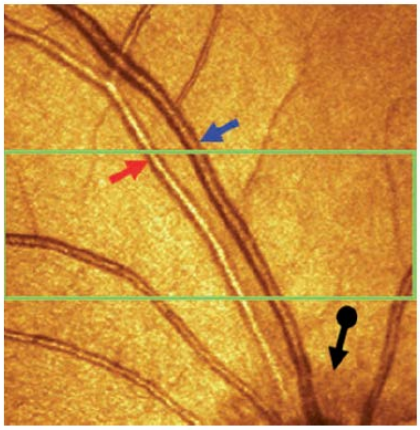

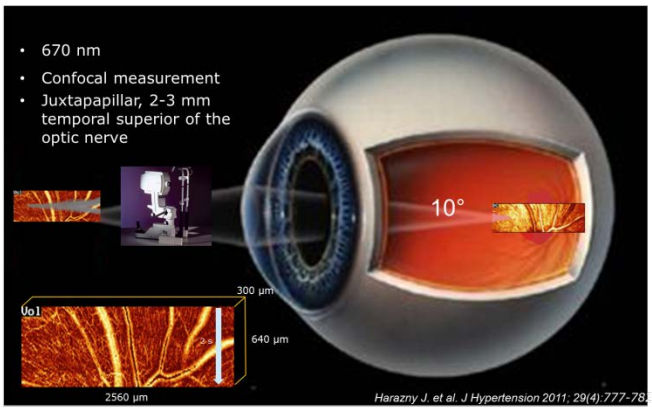

References:

1. Ott, C, Raff, U, Harazny, JM, Michelson, G, Schmieder, RE. Central pulse pressure is an independent determinant of vascular remodeling in the retinal circulation. **Hypertension.** 2013;61:1340-1345.
2. Jumar, A, Ott, C, Kistner, I, Friedrich, S, Michelson, G, Harazny, JM, Schmieder, RE. Early Signs of End-Organ Damage in Retinal Arterioles in Patients with Type 2 Diabetes Compared to Hypertensive Patients. **Microcirculation.** 2016;23:447-455.
3. Jumar, A, Ott, C, Kistner, I, Friedrich, S, Schmidt, S, Harazny, JM, Schmieder, RE. Effect of aliskiren on vascular remodelling in small retinal circulation. **J Hypertens.** 2015;33:2491-2499.
4. Harazny, JM, Raff, U, Welzenbach, J, Ott, C, Ritt, M, Lehmann, M, Michelson, G, Schmieder, RE. New software analyses increase the reliability of measurements of retinal arterioles morphology by scanning laser Doppler flowmetry in humans. **J Hypertens.** 2011;29:777-782.
5. Harazny, JM, Ritt, M, Baleanu, D, Ott, C, Heckmann, J, Schlaich, MP, Michelson, G, Schmieder, RE. Increased wall:lumen ratio of retinal arterioles in male patients with a history of a cerebrovascular event. **Hypertension.** 2007;50:623-629.
6. Jumar, A, Harazny, JM, Ott, C, Kistner, I, Friedrich, S, Schmieder, RE. Improvement in Retinal Capillary Rarefaction After Valsartan Treatment in Hypertensive Patients. **J Clin Hypertens (Greenwich).** 2016;18:1112-1118.
7. Rizzoni, D, Porteri, E, Boari, GE, De Ciuceis, C, Sleiman, I, Muiesan, ML, Castellano, M, Miclini, M, Agabiti-Rosei, E. Prognostic significance of small-artery structure in hypertension. **Circulation.** 2003;108:2230-2235.
8. Ritt, M, Schmieder, RE. Wall-to-Lumen Ratio of Retinal Arterioles as a Tool to Assess Vascular Changes. **Hypertension.** 2009;54:384-387.

3.3.Retinal intercapillary distance

Both parameters of capillary rarefication, i.e. measurement of intercapillary distance (ICD) and capillary area (CapA), are determined from perfusion images of pixels and have been previously described in detail. ICD is defined as distance between any pixel outside and the next pixel inside the vessel and expressed in µm. One pixel is defined as the smallest dot of optic solution, where flow can be detected. CapA is defined as area with predominance of vessels with ≤20 µm diameter and is given in number of pixels. Reliability of measurements have been previously shown to be fair (coefficient of variation <10%).

SLDF optic solution works in a confocal manner with pixel sizes of 10 x 10 µm. Pixels are located in a depth of 300 µm. Depending on the vessel size, pixels were categorized the following way: Pixels inside vessels > 20 µm were defined as non-capillary vessel pixels (e.g. arteriolar pixels),

pixels inside vessel 20 µm were defined as capillary pixels, and pixels outside a vessel were defined as intercapillary pixels.

For example:

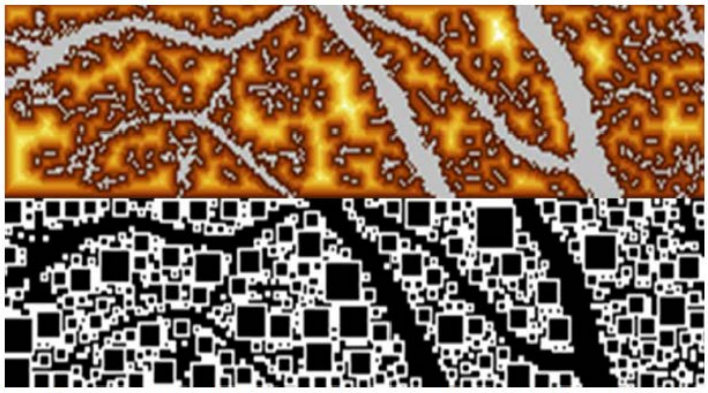

Fig 1. Measurement of intercapillary distance in perfusion image with scanning laser Doppler flowmetry and calculation of intercapillary distance using automatic full field perfusion image analyser

doi:10.1371/journal.pone.0162608.g001

References:

1. Harazny, JM, Ritt, M, Baleanu, D, Ott, C, Heckmann, J, Schlaich, MP, Michelson, G, Schmieder, RE. Increased wall:lumen ratio of retinal arterioles in male patients with a history of a cerebrovascular event. **Hypertension.** 2007;50:623-629.
4. Jumar, A, Harazny, JM, Ott, C, Kistner, I, Friedrich, S, Schmieder, RE. Improvement in Retinal Capillary Rarefaction After Valsartan Treatment in Hypertensive Patients. **J Clin Hypertens (Greenwich).** 2016;18:1112-1118.

4. Body composition measurements

Fluid status will be measured with a portable whole-body bioimpedance spectroscopy device (BCM, Fresenius Medical Care, Bad Homburg, Germany). Electrodes are attached to the hand and foot on the nondominant side of the body and electrical responses at 50 different frequencies between 5 and 1000kHz are measured. From the resulting impedance data and additional clinical parameters, extracellular water, intracellular water and total body water are calculated by the equations proposed by Moissl et al.

Fluid status assessed by the BCM is represented as “overhydration” (in Liter), based on a three-compartment model developed by Chamney et al. The three compartments are lean tissue mass, adipose tissue mass, and overhydration. Overhydration is the difference between the amount of extracellular water in the tissue actually detected by the BCM and the amount of water present in tissue predicted using physiological models under normal (euvolemic) conditions.

References:

1. Bley, TA, Wieben, O, Francois, CJ, Brittain, JH, Reeder, SB. Fat and water magnetic resonance imaging. **J Magn Reson Imaging.** 2010;31:4-18.
2. Moissl, UM, Wabel, P, Chamney, PW, Bosaeus, I, Levin, NW, Bosy-Westphal, A, Korth, O, Muller, MJ, Ellegard, L, Malmros, V, Kaitwatcharachai, C, Kuhlmann, MK, Zhu, F, Fuller, NJ. Body fluid volume determination via body composition spectroscopy in health and disease. **Physiol Meas.** 2006;27:921-933.
3. Chamney, PW, Wabel, P, Moissl, UM, Muller, MJ, Bosy-Westphal, A, Korth, O, Fuller, NJ. A whole-body model to distinguish excess fluid from the hydration of major body tissues. **Am J Clin Nutr.** 2007;85:80-89.

5. Estimate of Beta cell mass (Glucagon test)

In addition to insulin resistance, insufficient insulin secretion (for a given degree of insulin resistance) is a key factor that ultimately results in hyperglycemia. Among others, therapeutic approaches aiming to preserve beta-cell function or even restore beta-cell mass have therefore gained widespread attention over the past years. However, because functional beta-cell mass cannot be directly measured in vivo in humans, indirect methods that evaluate the beta-cell function are used instead. A good assessment of beta-cell function requires an evaluation of the dynamic insulin secretory capacity to a secretory stimulus. For practical reason, intravenous stimulation (e.g. with glucagon) is used. In a human study using tissue from patients who underwent pancreatectomy, the change of C-peptide by glucagon-test was the most valuable index of predicting functional beta-cell mass. Because glucagon directly stimulates beta-cells , the change of C-peptide concentrations by the glucagon-test is a valid index of secretory capacity of beta-cells, reflecting functional beta-cell mass.

Insulin secretion is measured in patients being fasting overnight [3]. For this purpose, blood samples are taken at 10 and 5 minutes and immediately prior (the mean of these 3 baseline measurements is calculated) to the intravenous administration of 1 mg glucagon (NovoNordisk A/S, Bagsvaerd, Denmark) as well as 6 minutes thereafter.

Using standardized laboratory methods, C-peptide, proinsulin and insulin (all Mercodia AB, Uppsala, Sweden) will be measured. In addition, insulin sensitivity index using HOMA-IR is calculated as fasting plasma glucose x fasting plasma insulin / 405 [4].

1. Fujita, Y, Kozawa, J, Iwahashi, H, Yoneda, S, Uno, S, Yoshikawa, A, Okita, K, Eguchi, H, Nagano, H, Imagawa, A, Shimomura, I. Increment of serum C-peptide measured by glucagon test closely correlates with human relative beta-cell area. **Endocr J.** 2015;62:329-337.
2. Samols, E, Marri, G, Marks, V. Promotion of Insulin Secretion by Glucagon. **Lancet.** 1965;2:415-416.
3. Ott C., Kistner I., Schmid A., Akarca E., Mahfoud F., Friedrich S., Ditting T., Veelken R., Böhm M., Uder M., Schmieder RE. Secretory capacity of pancreatic beta cells is enhanced 6 months after renal denervation in hypertensive patients. **Cardiovascular Diabetology**, 2018, submitted.
4. Matthews, DR, Hosker, JP, Rudenski, AS, Naylor, BA, Treacher, DF, Turner, RC. Homeostasis model assessment: insulin resistance and beta-cell function from fasting plasma glucose and insulin concentrations in man. **Diabetologia.** 1985;28:412-419.

6. Tissue sodium (^{23}Na-MRI) measurements [cooperation with the Diagnostic Institute of Radiology]

In brief, sodium content in muscle and skin of the lower leg can be measured with a ^{23}Na volume-coil (Stark-Contrast, Erlangen, Germany) at 3.0 T with a MRI scanner (Magnetom-Verio, Siemens Healthcare, Erlangen, Germany) using a 2D-FLASH sequence (total acquisition time, TA=13.7 minutes; echo time, TE=2.07 ms; repetition time, TR=100 ms; flip angle, FA=90°; 128 averages, resolution: 3×3×30 mm3). Four tubes containing aqueous solutions with 10, 20, 30, and 40 mmol/L NaCl serve as calibration standards by relating intensity to a concentration in a linear trend analysis. In parallel, we quantify tissue water content by ^{1}H-MRI, using a fat-saturated inversion recovery sequence with spin density contrast (inversion time, TI=210 ms; TA=6.29 minutes; TE=12 ms; TR=3 s; FA1/2=90°/180°; 128 averages, resolution: 1.5×1.5×5 mm3). The 10 mmol/L NaCl tube serves as a calibration standard for tissue water. For the analysis of the same image between 3-5 different readers, we found an excellent coefficient of variation (CV) of 1.0%-3.6% for results on skin sodium and 0.4%-0.7% for results on muscle sodium (intra-reader variability).

It is already observed that sodium content is significantly increased with aging, severe hypertension or hyperaldosteronism. This comprises tissue sodium content that encompasses both intra- and extracellular sodium signals. The current methodology cannot separate intracellular from extracellular sodium signals, but of note a close relationship to “dry sodium content” has been found.

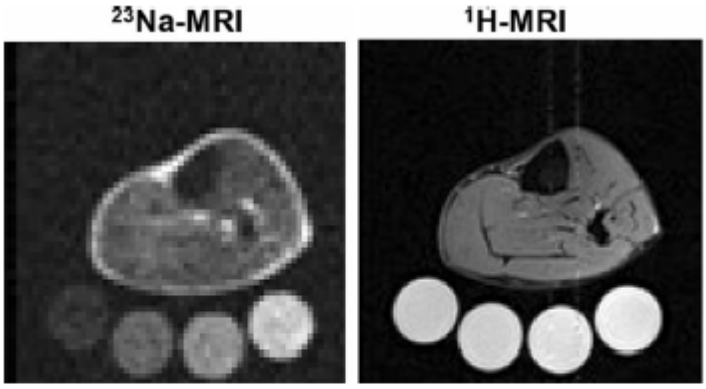

Fig. 1 *Left* Representative ^{23}Na magnetic resonance imaging (MRI) of the lower leg. Tubes (arranged *below*) contained solutions with 10, 20, 30, and 40 mmol/L of Na^+, hence serving as calibration standards by relating intensity to a concentration in a linear trend analysis. *Right* Tissue water content in the same patient assessed by ^{1}H-MRI

Risks of ^{23}Na-MRI/^{1}H-MRI assessments

Measurement of skin sodium content by ^{23}Na-MRI/^{1}H-MRI is a non-invasive method that is well established in the investigators clinical research unit (CRC) for several years. Due to its non-invasive nature and to our knowledge and long standing experience, there are no side effects. Of note, no contrast medium is applied.

References:

1. Kopp, C, Linz, P, Dahlmann, A, Hammon, M, Jantsch, J, Muller, DN, Schmieder, RE, Cavallaro, A, Eckardt, KU, Uder, M, Luft, FC, Titze, J. 23Na magnetic resonance imaging-determined tissue sodium in healthy subjects and hypertensive patients. **Hypertension.** 2013;61:635-640.
2. Hammon, M, Grossmann, S, Linz, P, Kopp, C, Dahlmann, A, Garlichs, C, Janka, R, Cavallaro, A, Luft, FC, Uder, M, Titze, J. 23Na Magnetic Resonance Imaging of the Lower Leg of Acute Heart Failure Patients during Diuretic Treatment. **PLoS One.** 2015;10:e0141336.
3. Kopp, C, Linz, P, Wachsmuth, L, Dahlmann, A, Horbach, T, Schofl, C, Renz, W, Santoro, D, Niendorf, T, Muller, DN, Neininger, M, Cavallaro, A, Eckardt, KU, Schmieder, RE, Luft, FC, Uder, M, Titze, J. (23)Na magnetic resonance imaging of tissue sodium. **Hypertension.** 2012;59:167-172.
4. Dahlmann, A, Dorfelt, K, Eicher, F, Linz, P, Kopp, C, Mossinger, I, Horn, S, Buschges-Seraphin, B, Wabel, P, Hammon, M, Cavallaro, A, Eckardt, KU, Kotanko, P, Levin, NW, Johannes, B, Uder, M, Luft, FC, Muller, DN, Titze, JM. Magnetic resonance-determined sodium removal from tissue stores in hemodialysis patients. **Kidney Int.** 2015;87:434-441.
5. Schneider, MP, Raff, U, Kopp, C, Scheppach, JB, Toncar, S, Wanner, C, Schlieper, G, Saritas, T, Floege, J, Schmid, M, Birukov, A, Dahlmann, A, Linz, P, Janka, R, Uder, M, Schmieder, RE, Titze, JM, Eckardt, KU. Skin Sodium Concentration Correlates with Left Ventricular Hypertrophy in CKD. **J Am Soc Nephrol.** 2017;28:1867-1876.
6. Karg, MV, Bosch, A, Kannenkeril, D, Striepe, K, Ott, C, Schneider, MP, Boemke-Zelch, F, Linz, P, Nagel, AM, Titze, J, Uder, M, Schmieder, RE. SGLT-2-inhibition with dapagliflozin reduces tissue sodium content: a randomised controlled trial. **Cardiovascular Diabetology.** 2018;17:5.
7. Kannenkeril, D, Karg, MV, Bosch, A, Ott, C, Linz, P, Titze, J, Nagel, AM, Uder, M, Schmieder, RE. Tissue Sodium Content in Patients with Type 2 Diabetes mellitus. **Diabetes and Vascular Disease Research.** 2018:submitted.
8. Kopp C, Linz P, Maier C, Wabel P, Hammon M, Nagel AM, Rosenhauer D, Horn S, Uder M, Luft FC, Titze J, Dahlmann A. Elevated tissue sodium deposition in patients with type 2 diabetes on hemodialysis detected by 23Na magnetic resonance imaging. **Kidney Int.** 2018 pii: S0085-2538(17)30857-8.

7. MRI arterial spin labeling [cooperation with the Diagnostic Institute of Radiology]

Arterial spin labeling (ASL) is performed with a 1.5 Tesla MRI scanner (Magnetom Aera, Siemens, Erlangen, Germany) using a FAIR True-FISP sequence. The FAIR and true fast imaging with steady state precession (True-FISP) approach combines a FAIR perfusion preparation and a True-FISP data acquisition strategy. The perfusion measurement is based on 2 data acquisitions, one with a global inversion prepulse, followed by one with a slice selective inversion (FAIR). The prepulses lead to a labeling of blood water spins. In contrast to the global inversion prepulse, the slice selective inversion prepulse only labels the blood water spins inside the kidney but not the inflowing blood water spins. Subtraction of both images therefore reflects the local perfusion. A 3rd image without the FAIR preparation pulse is measured to normalize the signal intensities on each patient. The technical and theoretical background of the sequence has been previously described in detail.

MRI is illustrated in Figure 1. Patients are examined in the supine position with a body-phased array coil (Siemens, Erlangen, Germany) in combination with a spine coil (Siemens, Erlangen, Germany). The FAIR True-FISP parameters included the following: repetition time, 4.9 ms; echo time, 2.5 ms; effective inversion time, 1200 ms; flip angle, 708; field of view, 360 mm; and in-plane resolution, 2.3 1.2 mm. All images were measured during expiration in breath hold. Breath-hold time was 18 seconds. Slices were positioned in an oblique coronal orientation to match the longitudinal axis of both kidneys. Slice thickness was 8 mm. Care was given to similarly position the slices in all subjects, and crucial attention was made to match the same slice position in both study time points within one subject.

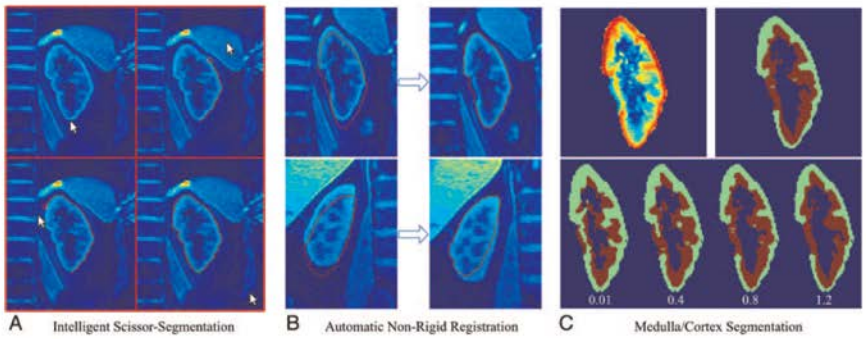

FIGURE 1. Processing of the images (from left to right). First, a semiautomatic segmentation using intelligent scissors is performed (A). The resulting contour is registered onto all images of 1 series using nonrigid registration (B). By evaluating the registration results we can distinguish a good (B, top) from a bad registration (B, bottom). Cortex/medulla segmentation was performed using a k-means clustering algorithm (C). This clustering is based on the averaged registered global inversion images (C, top left). To enable the user to modify the final medulla/cortex segmentation a parameter α is premultiplied to the gray values and directly influences the boundary between medulla and cortex result (c, bottom). In the assessed cases, the parameter α was set to 1.0 (c, top right). However, the adjustment of α may be beneficial in particular cases.

References

1. Hammon, M, Janka, R, Siegl, C, Seuss, H, Grosso, R, Martirosian, P, Schmieder, RE, Uder, M, Kistner, I. Reproducibility of Kidney Perfusion Measurements With Arterial Spin Labeling at 1.5 Tesla MRI Combined With Semiautomatic Segmentation for Differential Cortical and Medullary Assessment. **Medicine (Baltimore).** 2016;95:e3083.
2. Martirosian, P, Klose, U, Mader, I, Schick, F. FAIR true-FISP perfusion imaging of the kidneys. **Magnetic Resonance in Medicine.** 2004;51:353-361.
3. Ott C, Janka R, Schmid A, Titze S, Ditting T, Sobotka PA, Veelken R, Uder M, Schmieder RE. Vascular and renal hemodynamic changes after renal denervation. **Clin J Am Soc Nephrol.** 2013;8:1195-201.

4. Schneider MP, Janka R, Ziegler T, Raff U, Ritt M, Ott C, Veelken R, Uder M, Schmieder RE. Reversibility of the effects of aliskiren in the renal versus systemic circulation. **Clin J Am Soc Nephrol.** 2012;7:258-64.
5. Ritt M, Janka R, Schneider MP, Martirosian P, Hornegger J, Bautz W, Uder M, Schmieder RE. Measurement of kidney perfusion by magnetic resonance imaging: comparison of MRI with arterial spin labeling to para-aminohippuric acid plasma clearance in male subjects with metabolic syndrome. **Nephrol Dial Transplant**. 2010;25:1126-33.

7.1.Renal cortical and medullar perfusion

Since we are especially interested in distinct cortex and medulla perfusion values, an additional segmentation step is required. For this purpose, we use the average over the registered global inversion images (Figure 1C, top left). In pretests, we identified the global inversion images to show the best separation of gray values between calyces, medulla, cortex, and background. To separate these regions, we use a k-means clustering method on the pixel gray values. For increased robustness, we extended this gray value based approach by adding the distance to the kidney's center of gravity into the computation. This leads to coherently segmented regions and finally to a more robust and correct registration (Figure, top right). To enable the user to modify the final medulla/cortex segmentation a parameter a is premultiplied to the gray values and directly influences the boundary between medulla and cortex (Figure, bottom). In the assessed cases, a was set to 1.0. However, the adjustment of this parameter may be beneficial in special cases. A morphological filter is used to ensure that no medullar or background pixels remain in the region of the segmented cortical area. Although this may lead to a slightly under-segmented cortex, the segmentation is guaranteed to only contain pixels completely belonging to the cortex.

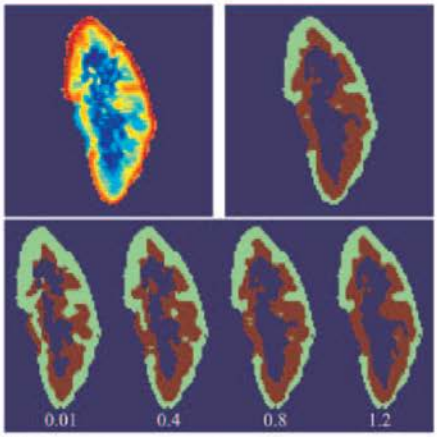

C Medulla/Cortex Segmentation

The final image analysis in our experiments was always based on 8 acquired global/slice inversion image pairs and 1M0 image. These images were segmented and registered using the previously described algorithm. Bad image pairs can be sorted out immediately by the registration software. We evaluated different computation schemes and settled on computing a perfusion image for every acquired image pair. From the image pairs showing a good registration, we used the 4 pairs showing the highest perfusion values. Taking the average over these perfusion images showed the best reproducibility, while maintaining a good separation between patients with different kidney functions.

References:

1. Hammon, M, Janka, R, Siegl, C, Seuss, H, Grosso, R, Martirosian, P, Schmieder, RE, Uder, M, Kistner, I. Reproducibility of Kidney Perfusion Measurements With Arterial Spin Labeling at 1.5 Tesla MRI Combined With Semiautomatic Segmentation for Differential Cortical and Medullary Assessment. **Medicine (Baltimore).** 2016;95:e3083.